Human Cone Visual Pigment Deletions Spare Sufficient Photoreceptors to Warrant Gene Therapy

Artur V. Cideciyan,[1*] Robert B. Hufnagel,[2*] Joseph Carroll,[3] Alexander Sumaroka,[1] Xunda Luo,[1] Sharon B. Schwartz,[1] Alfredo Dubra,[3] Megan Land,[3] Michel Michaelides,[4] Jessica C. Gardner,[4] Alison J. Hardcastle,[4] Anthony T. Moore,[4] Robert A. Sisk,[2] Zubair M. Ahmed,[2] Susanne Kohl,[5] Bernd Wissinger,[5¶] and Samuel G. Jacobson[1¶]

[1]Scheie Eye Institute, Department of Ophthalmology, University of Pennsylvania Perelman School of Medicine, Philadelphia, PA, USA; [2]Divisions of Human Genetics and Pediatric Ophthalmology, Cincinnati Children's Hospital, and Cincinnati Eye Institute, Cincinnati, OH, USA; [3]Departments of Ophthalmology, Cell Biology, Neurobiology, and Anatomy, and Biophysics, Medical College of Wisconsin, Milwaukee, WI, USA; [4]UCL Institute of Ophthalmology and Moorfields Eye Hospital, London, United Kingdom; [5] Molecular Genetics Laboratory, Institute for Ophthalmic Research, Centre for Ophthalmology, University Tuebingen, Tuebingen, Germany.

*First two authors contributed equally.

[¶]Co-corresponding authors:
S.G. Jacobson, Scheie Eye Institute, University of Pennsylvania, 51 N. 39th Street, Philadelphia, PA 19104, USA.
Tel: +1 215 662 9981; Fax: +1 215 662 9388;
Email: jacobsos@mail.med.upenn.edu
And
B. Wissinger, Molecular Genetics Laboratory, Institute for Ophthalmic Research, Centre for Ophthalmology, University Tuebingen, Roentgenweg 11, 72076 Tuebingen, Germany.
Tel: +49 7071 29 80702; Fax: +49 7071 29 5725;
E-mail: wissinger@uni-tuebingen.de

Abstract

Human X-linked blue-cone monochromacy (BCM), a disabling congenital visual disorder of cone photoreceptors, is a candidate disease for gene augmentation therapy. BCM is caused by either mutations in the red (*OPN1LW)* and green (*OPN1MW)* cone photoreceptor opsin gene array or large deletions encompassing portions of the gene array and upstream regulatory sequences that would predict a lack of red or green opsin expression. The fate of opsin-deficient cone cells is unknown. We know that rod opsin null mutant mice show rapid postnatal death of rod photoreceptors. We studied a cohort of 20 BCM patients (ages 5-58) with large deletions in the red/green opsin gene array using *in vivo* histology with high resolution retinal imaging. Already in the first years of life, retinal structure was not normal: there was partial loss of photoreceptors across the central retina. Remaining cone cells had detectable outer segments that were abnormally shortened. Adaptive optics imaging confirmed existence of inner segments at a spatial density greater than that expected for the residual blue cones. The evidence indicates that human cones in patients with deletions in the red/green opsin gene array can survive in reduced numbers with limited outer segment material, suggesting potential value of gene therapy for BCM.

Introduction

The human retina has on average 100 million rod photoreceptors that subserve night vision and six million cone photoreceptors responsible for daylight, color and fine spatial vision (Osterberg, 1935; Curcio *et al.,* 1990). Three cone photoreceptor types with light-absorbing visual pigments of different wavelength sensitivity - named simply blue (short-wavelength sensitive, S), green (middle-wavelength sensitive, M) and red (long-wavelength sensitive, L) – give rise to trichromacy of normal human color vision (Young, 1802; Helmholtz, 1866). The apoprotein opsins of rods and three types of cones are integral membrane proteins in the photoreceptor outer segments. Four kinds of pigments are thus formed when opsins are covalently linked to the 11-*cis*-retinal chromophore. Light absorbed by the pigments leads to isomerization of 11-*cis* to all-*trans* retinoid; the phototransduction cascade is activated in the corresponding rod or cone cell; and visual perception begins. At least two visual (retinoid) cycles are responsible for recycling the all-*trans*-retinal back to the 11-*cis* configuration in order to recharge the rod and cone pigments for continued vision (Nathans *et al.,*1986a,b; Saari, 2000; Palczewski, 2010; Neitz and Neitz, 2011; Wang and Kefalov, 2011).

The three cone subtypes differ in numbers and spatial distribution in adult human retina (Hofer *et al*., 2005). L and M cones are the most populous and peak density is in the fovea, the very central retina; S cones are only about 2-7% of the total cone population (Curcio *et al*., 1990; Curcio *et al.,* 1991; Mustafi *et al*., 2009). The gene encoding S cone opsin (*OPN1SW)* is located on chromosome 7q31.3-q32. *OPN1LW* and *OPN1MW*, encoding the L and M cone opsins, respectively,

are located on Xq28 and arranged as a head-to-tail tandem array and expression is driven and regulated by specific promoters and a single upstream locus control region (LCR) (Nathans *et al.,*1986a,b; Neitz and Neitz, 2011).

X-linked eye disorders resulting from mutations in the L/M cone opsin gene array range from common color vision deficiencies to severe loss of day vision with nystagmus and macular degeneration (Nathans *et al.,*1986a; Nathans *et al.,* 1989; Neitz and Neitz, 2011) . The latter disorder, named blue-cone monochromacy (BCM; OMIM #303700), is associated with three categories of mutations affecting *OPN1LW* and *OPN1MW* loci. Recent imaging analyses of the retina in subjects with two of the mutation types (missense mutations and L/M interchange mutations) reported differences in disease expression between them and raised potential issues with their candidacy for visual restoration by gene augmentation therapy (Carroll *et al*., 2012). The third category involving large deletions of the L/M pigment genes and/or deletions upstream of the L pigment gene containing the LCR, however, were not studied with modern methods. These mutations would be expected to result in complete absence of L/M cone opsin expression (Wang *et al*., 1992). A clue about possible effects of such mutations came with the finding of abnormal cone mosaics in carrier females (Carroll *et al*., 2010). We evaluated the retinal structure and function in BCM caused by such large deletion mutations, and weighed the value and goals of gene augmentation as a therapy for such patients.

Materials and Methods

Human subjects

Twenty patients (ages 5 to 58 years) with a clinical diagnosis of BCM and mutations in the X-chromosome visual pigment genes were included (Table 1). Informed consent or assent was obtained; procedures followed the Declaration of Helsinki and had institutional review board approval. All patients underwent a complete eye examination, genetic analyses as well as specialized tests of retinal cross-sectional structure; subsets of patients were imaged with AOSLO or evaluated with specialized visual function tests.

Genetic analyses

Whole venous blood samples were collected and genomic DNA extracted according to standard procedures. Details are provided in Supplementary Methods.

En face autofluorescence imaging and in vivo microscopy of human retina

Health of the retinal pigment epithelium (RPE) was evaluated with reduced-illuminance autofluorescence imaging (RAFI) as published (Cideciyan *et al*., 2007). Near-infrared (NIR) excitation was used to detect melanin granules and short-wavelength (SW) excitation was used to detect lipofuscin granules (Cideciyan *et al*., 2007; Gibbs *et al*. 2009). Cross-sectional images of the retina were obtained with a spectral-domain optical coherence tomography (SD-OCT) instrument (RTVue-100, Optovue Inc., Fremont, CA). Details are provided in Supplementary Methods.

Adaptive optics imaging of the photoreceptor mosaic

A previously described adaptive optics scanning laser ophthalmoscope (AOSLO) was used to image each subject's photoreceptor mosaic (Dubra *et al*., 2011). Details are provided in Supplementary Methods.

Spectral sensitivity function

Spectral sensitivity functions were measured in normal subjects (n=3, ages 31-50) and BCM P15 using a modified perimeter with methods previously described (Cideciyan *et al*., 1998). Details are provided in Supplementary Methods.

Results

Genetic findings and clinical characteristics of the BCM patients

Pedigrees of the 11 families in this study suggested X-linked inheritance (Fig.1A). The clinical diagnosis of all 20 patients was BCM. From early life, there was reduced visual acuity and nystagmus. When there was more specific information (by history) of age of onset or a decline or an increase in nystagmus, this was noted (Table 1). All but 3 of the patients described light aversion to some degree, leading to coping strategies such as almost continuous wear of sunglasses or squinting. Color vision was abnormal indicating cone dysfunction, but there was detectable S cone function. Electroretinography (ERG) revealed normal or nearly normal rod signals but severely abnormal cone ERGs (Table 1). Genetic analyses identified genomic deletions of various extents at the

OPN1MW/*OPN1LW* gene cluster in all 20 BCM patients (Fig.1B). In 10 of the families, the deletions encompassed the LCR as well as the *OPN1LW* promoter. In Family 1, the LCR region was intact but a large (over 45.5 kb) deletion covered all coding exons of the *OPN1LW* gene as well as the promoter and first coding exon of the *OPN1MW* gene (Fig.1B). The types of deletions represented in the 11 families are considered sufficient for the complete loss of expression of the *OPN1MW*/*OPN1LW* genes on the X-chromosome (Wang *et al*., 1992).

Near normal retinal-macular appearance by en face viewing in most BCM eyes

The traditional clinical view is that BCM is a congenital cone vision disturbance with normal retinal appearance in early life but the possibility of macular degeneration later in life (Weleber, 2002). *En face* imaging, performed with reduced-illuminance autofluorescence imaging (RAFI) methods (Cideciyan *et al*., 2007), confirmed this clinical impression in our BCM cohort (Fig.2A). RAFI assays the health of the retinal pigment epithelium (RPE) - the cellular layer adjacent to the photoreceptors - taking advantage of its naturally-occurring fluorophores melanin and lipofuscin excited by near-infrared (NIR) and short-wavelength (SW) lights (Gibbs *et al*., 2009). P1 (age 8) represents the majority of BCM patients who showed a macular appearance indistinguishable from normal with its characteristic higher central intensity on NIR-RAFI and lower central intensity on SW-RAFI (Fig.2A). P16 (age 28) together with two other BCM patients (P19,P20; ages 43,55) represent a second group with minor abnormalities consisting of a lack of a distinct foveal hypo-autofluorescence on SW-RAFI and/or

heterogeneity on NIR-RAFI (Fig.2A). P4 (age 50) was the only BCM patient in this cohort showing a distinct region of foveal RPE atrophy apparent on both imaging modalities.

Cone photoreceptor cells in BCM diminished already in childhood

Using retinal cross-sectional imaging, we examined the hypothesis that BCM is simply an early-onset cone visual disturbance and only older patients may show macular atrophy. The layer corresponding to photoreceptor nuclei was measured to determine if the photoreceptor cells were intact (Fig.2B-E). Scans crossing the fovea along the vertical meridian are shown in a representative normal subject and three BCM patients (Fig.2B). The photoreceptor outer nuclear layer (ONL) layer, which includes the photoreceptor nuclei and their axons (Lujan *et al.*, 2011) is highlighted. P1 (age 5) and P16 (age 28) showed some differences from the normal (age 29), whereas P4 (age 50) had foveal degeneration with a ~2 mm region missing all photoreceptor nuclei (Fig.2B). Quantitation of ONL thickness in all BCM patients indicated there was a central region of abnormal thinning surrounded by normal or near normal thickness at greater eccentricities (Fig.2C). At the foveola, which normally is dominated by L/M cones and lacks rods (Borwein *et al.*, 1980; Youdelis and Hendrickson, 1986), the ONL was abnormally thin in all patients but one (Fig.2D, upper panel). Younger BCM patients between the ages of 5 and 20 showed a mean foveolar ONL thickness of 60.7 μm (SD=13 μm; n=12) which is about 60% of normal (mean±SD, 95.7±9.5 μm; n=22, ages 8-62). Older BCM patients, with some exceptions, tended to show increased thinning

of foveolar ONL with age (Fig.2D, upper panel). In a subset of 8 patients (P1-P4,P7-P10), longitudinal data spanning 2 to 9 years (mean, 5 y) was suggestive of a slowly progressive disease averaging 11.9 μm/decade thinning of the ONL at the foveola.

Immediately surrounding the foveola (~0.8 mm eccentric), rod as well as cone nuclei normally occupy the ONL. All but the youngest patients showed abnormal ONL thickness at this location (Fig.2D, middle panel) implying potential involvement of macular rods in addition to cones in the BCM pathology. The highest density of rods in the human retina is located outside the macula at the 'rod hot spot' in the superior retina (~3.5 mm from the foveola), and the ONL at this location is expected to be dominated by rod photoreceptor nuclei (Curcio *et al*., 1990). All BCM patients had normal ONL thickness in this rod-dense zone (Fig.2D, lower panel). When the spatial extent of the central retinal region with abnormal ONL thickness was quantified along the vertical meridian, there was an age-related expansion from ~3 mm extent (corresponding to ~1.5 mm eccentricity) in the first decade of life to ~4 mm extent in the 4th decade of life (Fig.2E). Assuming circularly isotropic distribution, the ONL abnormality would be expected to cover a substantial proportion of the macula (Fig.2E, inset).

Abnormal but detectable cone photoreceptor outer segments in BCM

Is the BCM disease sequence like that in human *rhodopsin* (rod opsin) mutations with photoreceptor outer segment shortening accompanying or

preceding the cell loss (Milam *et al*., 1998)? The answer was sought by analyses of the optical coherence tomography (OCT) signals originating from subcellular components of photoreceptors in our BCM cohort.

In the normal central retina immediately eccentric to the foveola, there are five distinct hyperscattering peaks (Srinivasan *et al*., 2008; Sakami *et al.,* 2011; Mustafi *et al.,* 2011; Kocaoglu *et al.,* 2011; Spaide and Curcio, 2011; Syed *et al*., 2013) (Fig.3A). These peaks are thought to correspond to the outer limiting membrane (OLM), ellipsoid region of photoreceptor inner segments (ISe), the contact cylinder between the RPE apical processes and the cone OS tips (COST), apical RPE microvilli and rod outer segment tips (ROST), and basal RPE and Bruch's membrane (RPE/BrM). Comparison of the longitudinal reflectivity profiles (LRPs), the signal underlying the scans, with a previously published model using quantitative histological measurements (redrawn from Spaide and Curcio, 2011) shows the expected correspondence of scattering peaks and subcellular rod and cone structures at 0.5 and 0.8 mm superior to the foveola (Fig.3C).

The BCM foveola often shows discrete discontinuities along the ISe band, suggesting abnormality at the inner and outer segment regions of the photoreceptor cells (Fig.3B, arrowhead). Existence of these cavitations (Carroll *et al*., 2012; Leng *et al*., 2012) does not allow quantitative analyses to be performed in some of the patients at the foveola. Thus, LRPs were analyzed first at 0.5 and 0.8 mm superior to the foveola (Fig.3B,D). These locations are still within the foveal region of the human macula. At 0.5 and 0.8 mm, all BCM patients showed hyperscattering peaks identifiable as OLM, ISe, ROST and RPE/BrM. In addition,

the majority of BCM patients, exemplified by P9, showed an intermittently identifiable hyperscattering peak (Fig.3B, dashed orange bands between ISe and ROST). This peak is where the COST peak would be expected. A model of the BCM retina at the level of the photoreceptor inner and outer segments (using the identities of hyperscattering peaks derived from normal retina) schematizes the interpretation most consistent with the data at the 0.5 and 0.8 mm superior loci (Fig.3D). The distance from the ISe peak to the COST peak, representing the length of cone outer segments (COS), was quantifiable in many BCM patients. At 0.5 mm eccentricity, the mean COS length in BCM was 11.2 μm (SD=2.4 μm; n=12) representing ~40% of normal value (28.1±2.1 μm) (Fig.3E). At 0.8 mm eccentricity, the mean COS length in BCM was 10.0 μm (SD=3.1 μm; n=13) representing ~41% of the normal value (24.2±2.7 μm) (Fig.3F). There was no obvious relationship between COS length and age at either eccentricity (Fig.3E,F). In some BCM patients, a COST peak may not have been identifiable either because of a lack of cones or because COS were shorter than the axial resolution of the instrument. There was no obvious age relationship to the identifiability of the COST peak; there were both younger and older patients without a COST peak.

Abnormally short rod photoreceptor outer segments in BCM

Rod and cone OS lengthening tend to be temporally synchronized during human retinal development (Hendrickson and Drucker, 1992). We questioned whether the abnormal congenital shortening of the COS in BCM patients could have secondary consequences on the developmental elongation of ROS length. The distance between hyperscattering LRP peaks ISe and ROST was used to estimate the ROS length in BCM (Fig.3A-D).

At 0.5 mm eccentricity, all BCM patients showed abnormally short ROS length; the mean was 26.1 μm (SD=4.5 μm; n=19) representing ~59% of normal (44.2±3.1 μm) (Fig.3G). Similarly at 0.8 mm eccentricity, the mean ROS length was 26.7 μm (SD=3.0 μm; n=19) representing ~65% of normal (41.0±2.9 μm) (Fig.3H). There was no obvious age relationship; both the youngest patients in the first decade of life as well as older patients in the fourth and fifth decades of life showed ROS length shortening of similar extent with the exception of P4, the patient with foveal atrophy. At 3.5 mm superior retina – a locus within the rod hot spot – ROS thickness straddled the lower limit of normal (71 to 90% of mean normal, data not shown) and again there was no obvious age relationship, except for P4.

'Dark' cones in BCM: remnant L/M cones with impaired reflectivity

To define the identity and spatial density of photoreceptors in BCM, AOSLO was used to image along a plane tangential to the retina at the level of the inner segments (Dubra *et al.*, 2011). The normal photoreceptor mosaic at 1.5 mm

eccentricity contains regularly-spaced larger and smaller structures (Fig.4A, left). Under high magnification (Fig.4C), the larger structures have a central reflective core surrounded by a darker ring, consistent with normally waveguiding and reflecting bright cones; and the smaller structures are consistent with adjacent rods (Dubra *et al*., 2011; Cooper *et al*., 2011; Carroll *et al*., 2012). The BCM patient P11 had a different pattern compared to normal at the same eccentricity (Fig.4A). Under high magnification, two types of larger structures with interleaving smaller structures could be distinguished in the BCM retina. Larger structures retaining a central reflective core would be consistent with normal waveguiding and reflecting bright cones, whereas larger structures missing the central reflective component would correspond to dark cones with present inner segments but missing, shortened or otherwise abnormal outer segments (Fig.4C). The altered outer segment morphology would be expected to interfere with normal waveguiding and/or reflection of light. The smaller structures are presumed to be rods. Closer to the foveola, at 0.8 and 0.5 mm, the mosaics of BCM patients P6 and P11 showed a similar pattern to each other and to the images at 1.5 mm consisting of bright and dark cones, and interleaved rods (Fig.4B,C) that appeared larger in diameter than normal rods and more distinct. Taken together with the evidence of shortened COS length (Fig.3) and the underlying molecular defect in L/M cone opsin, a parsimonious hypothesis is that in BCM the bright cones represent the S cone population whereas the dark cones represent remnant L/M cones.

To support this interpretation, quantitative analyses of the spatial density of photoreceptors were performed at three eccentricities. At 1.5 mm, P11 had 85,734 rods/mm^2 which was normal by imaging (85,785 ± 14,914 rods/mm^2) as well as by published histology (94,079 rods/mm^2, Curcio *et al.*, 1990) (Fig.4D). At 0.8 and 0.5 mm, normal rod inner segments are difficult to distinguish individually by current non-invasive AOSLO imaging methods due to their size, packing and relatively wide reflectivity profile (Dubra *et al.*, 2011). Larger rod inner segments combined with lower cone densities in BCM allow quantitation of rod densities near the fovea in these subjects. Rod densities of P6 (62,812 and 57,344 rods/mm^2 at 0.8 and 0.5 mm, respectively) and P11 (70,156 and 53,594 rods/mm^2 at 0.8 and 0.5 mm, respectively) were normal or near normal based on published histology (73,600 and 51,853 rods/mm^2 at 0.8 and 0.5 mm, respectively, Curcio *et al.*, 1990).

The spatial density of all cones (both bright and dark) in BCM (4351 and 5128 cones/mm^2 in P6 at 0.8 and 0.5 mm, respectively; 4194, 4999 and 6065 cones/mm^2 in P11 at 1.5, 0.8 and 0.5 mm, respectively) were ~25 % of normal by imaging or by histology (Curcio *et al.*, 1990) (Fig.4D-F). Consistent with the assumption that a healthier S cone population corresponds to the bright cones in BCM, their spatial densities (1865 and 2486 cones/mm^2 in P6 at 0.8 and 0.5 mm, respectively; 1864, 2499 and 2022 cones/mm^2 in P11 at 1.5, 0.8 and 0.5 mm, respectively) were similar to that expected from a 7% estimate of the total cone population (Hofer *et al.*, 2005) imaged by AO or direct S cone density estimates from histology (Curcio *et al.*, 1991) (Fig.4D-F). Three other BCM patients (P12, P14, and P18) imaged with AOSLO had qualitatively similar findings, although

greater instability of fixation did not allow reconstruction of a wide angle montage required to make quantitative measurements at known retinal eccentricities. AOSLO imaging results taken together with OCT provided further evidence that BCM patients have a lower cone density than that seen in normals, but a higher total cone density than would be expected for just the S cone submosaic, indicating the existence of a remnant L/M cone population in BCM.

Retinal structure at the BCM foveola

The foveola refers to a region at the center of the fovea packed with L/M cones and lacking rod photoreceptors (Borwein *et al*., 1980; Youdelis *et al*., 1986). Foveola is thus a key retinal location to answer questions about L/M cones in BCM. On optical cross-section of the normal foveola, the number of hyperscattering peaks distinguishable distal to the hyposcattering ONL trough are reduced from five to four consistent with the lack of the ROST peak (Fig.5A); notably, this feature is only observed when the scan is obtained through the exact cone-only region. Comparison of the normal foveolar LRP with a previously published model using quantitative histological measurements (redrawn from Spaide and Curcio, 2011) shows the correspondence of scattering peaks and subcellular structures at the foveola (Fig.5C). The peaks are thought to correspond to the OLM, ISe, the interface at or near the apical RPE microvilli and COST, and the interface near the basal RPE and BrM.

Quantitative analyses of the foveola were possible in six BCM patients (P2, P6, P8, P11, P15 and P17; ages 8-33) that demonstrated a partially intact ISe

band at this location (Fig.3B). Similar to the 0.5 and 0.8 mm loci in BCM and normal subjects, but unlike the foveolar scans in normals, there were five hyperscattering peaks detectable at the foveola of these BCM patients. Of note was the small but identifiable hyperscattering peak immediately distal to ISe band in addition to the pair of larger hyperscattering peaks (Fig.5B). Such a scattering signature would be consistent with an admixture of cone photoreceptors with shorter COS as well as a second type of photoreceptors (likely rods) with longer outer segments (OS) (Fig.5D). In the six BCM patients with retained foveolar structure, the COS length ranged from 8.5 to 14.5 μm, which is ~30% of normal COS length at the foveola (38.1±2.7 μm). The longer OS length ranged from 21 to 35 μm (Fig.5E).

AOSLO images of the normal fovea show a contiguous mosaic of cones that decrease in diameter and increase in density towards the foveola (Fig.5F) as expected from cone packing (Curcio *et al.*, 1990). BCM patients showed a severely disrupted foveal mosaic, consisting of a ring of sparsely packed, highly reflective bright cones and a second population of weakly reflecting photoreceptors which were present throughout the foveola (Fig.5F). The bright cones presumably correspond to S cones and the central region lacking bright cones defines the extent of the S-cone free zone at the center of the foveola; this has been noted in other patients with BCM (Carroll *et al.*, 2012). The weakly reflecting cells may comprise both remnant L/M cones and rods, though it was not possible to differentiate subtypes within this population. The density of these cells

at the foveola (38,400 cells/mm^2 and 42,400 cells/mm^2 for P6 and P11, respectively) was ~25% of the normal (162,000 cells/mm^2).

Evidence for abnormal but detectable L/M cone function in BCM

Lastly we asked whether a subset of structurally retained L/M cones with shortened outer segments could make a contribution to visual perception in BCM patients. Visual function was assessed in P15 at fixation which was located at 0.6 mm supero-temporal to the foveola. P15 was able to view a bright ambient light without squinting. Many BCM patients squint in even modest lighting presumably in order to limit desensitization of their rods by ambient light levels.

Spectral sensitivity was determined under scotopic and photopic conditions. This was achieved by testing under dark-adapted as well as a range of ambient light conditions designed to increasingly desensitize the dominant rod photoreceptor function in order to uncover cone photoreceptor function (Fig.5G). Under scotopic conditions, normal and BCM vision were spectrally consistent with rod photoreceptor mediation (Fig.5G, far left panel). Under low photopic (mesopic) conditions using a dim (1 cd.m^{-2}) achromatic background light, sensitivities in normal subjects are mediated by S cones and L/M cones when probed with short-, middle- and long-wavelength stimuli, respectively. In BCM P15 under low photopic conditions, sensitivity was mediated by S cones and rods; there was no spectral evidence of L/M cone function. Under higher photopic conditions, sensitivities in normal subjects were dominated by S and L/M cones when probed with short- and long-wavelength stimuli, respectively. In BCM P15, under photopic conditions,

spectral sensitivities again were consistent with S cone and rod function. Under high photopic conditions, however, the spectral sensitivity function of P15 was consistent with L/M cone function about 1.5 log units reduced compared to normal.

Discussion

Consequences of congenital cone opsin deficiency on cones

A congenital reduction in density or absence of rod opsin in the rod outer segment, as in the rhodopsin knockout mouse, causes loss of outer segment integrity and rapid rod cell death (Humphries *et al*., 1997; Lem *et al*., 1999; Liang *et al*., 2004; Makino *et al*., 2012). Should we expect the same consequences for L/M cone photoreceptors as for rods when there is congenital opsin deficiency, such as in BCM with large deletions at the *OPN1LW-OPN1MW* gene cluster? The many differences between structure and function of rods versus cones make such an extrapolation uncertain (Mustafi *et al*., 2009). Cones contain about half as many visual pigment molecules as do rods (Mustafi *et al*., 2009; Tachibanaki *et al*., 2001). Cones, in contrast to rods, do not have separate stacked membranous discs but have a lamellated continuously-connected membrane. The turnover rate of cone outer segments is thought to be less rapid than in rods (Mustafi *et al*., 2009; Jonnal *et al.,* 2010). The expectation is that the effects of opsin deficiency on cones could be different than on rods, and this has been bolstered by the clinical impression that BCM may simply be a congenital stationary cone dysfunction with some patients having a degenerative component in later life.

From the present studies of BCM, we know that there is not only severe congenital cone visual dysfunction but also a reduced number of cones even in the youngest patients studied (as early as age 5 years). Evidence of progressive central retinal cone loss was present in some patients and macular atrophy in later stages, thereby confirming previous observations (for example, Nathans *et al.,* 1999; Ayyagari *et al.,* 1999; Kellner *et al.,* 2004). This disease pattern does show some resemblance to that in the rhodopsin knockout mouse but it is less cataclysmic. The cone cell reduction detected in early life could represent the end of a rapid post-natal phase of degeneration, and this may be followed by a slowly progressive decades-long phase of further cone loss. Alternatively, congenital cone opsin deficiency may interfere with the protracted post-natal maturation of the human fovea and the BCM retinas may not complete normal high density cone packing in the fovea, which takes years to achieve (Hendrickson *et al*., 2012).

In BCM patients with normal retinal lamination at the foveola, there was evidence for some photoreceptors retaining outer segments. At least a subset of these photoreceptors likely corresponds to remnant L/M cones with abnormally shortened outer segments. A small number of rod cells with longer outer segments may also have migrated into the foveola during an incomplete foveal maturation process. Surrounding the foveola, there were shortened but detectable cone outer segments, corresponding to weakly-reflecting dark cone inner segments (Carroll *et al*., 2004; Cho *et al*., 2013). These likely represent remnant L/M cones. Also surrounding the foveola, intermingled with the cones, were slightly shortened rod outer segments and swollen rod inner segments; rod cell density was near normal.

It is tempting to attribute the minor rod inner and outer segment abnormalities in the central BCM retina to 'stress' from neighboring abnormal cones (Milam *et al*., 1998; Rossi *et al*., 2013), and to make analogies to the secondary cone loss known to occur in rod-specific diseases. The effects of rod loss on cones continue to be explored (Humphries et al., 2012) and a rod-derived cone viability factor has been identified (Leveillart and Sahel, 2010); but little is known of the effects of cone loss on rods. It is also possible that defective development is at play because the rod abnormalities are present as early as we measured (Hendrickson *et al.,* 2012).

Residual L/M cone function in BCM caused by a deletion at the L/M opsin gene cluster

Vision in BCM is classically dominated by rod and S cone photoreceptors (Blackwell and Blackwell, 1957; Blackwell and Blackwell, 1961; Nathans *et al*., 1989) but existence of a residual amount of L/M cone driven vision has been demonstrated in patients preceding the molecular era (Smith *et al*., 1983). Detailed visual function studies defining the extent of residual L/M cone function in molecularly-characterized patients have been rare. Consistent with the classical point of view has been the lack of detectable L/M cone function in three patients: one with a deletion genotype, and two patients with C203R missense mutations (52). On the other hand, residual L or M cone function was found in a 23-year-old patient with the LIAVA type of mutation (Crognale *et al.,* 2004), which is thought to cause abnormal splicing of exon 3 of the cone opsin gene (Ueyama *et al.,* 2012),

and in several young affected males in a family with a deletion genotype (Mizrahi-Meissonnier *et al*., 2010) very similar to the genotype of our Family 1. In patient P15, central vision was mediated by rods and S cones under dark-adapted or standard ambient light conditions. Upon desensitization of the rods by a brighter background light, however, residual vision originating from L/M cones was uncovered (Fig.5). Molecular analysis showed that this subject carries a deletion that encompasses the LCR and parts of the proximal L opsin gene. However, at least one intact M opsin gene with a functional proximal promoter is still present. We hypothesize that low levels of M opsin are expressed in this BCM patient's cone photoreceptors with abnormally shortened outer segments and this enables cone vision to be detected psychophysically.

Searching for an animal model with cone opsin deficiency and cone cell loss for proof-of-concept studies of therapy in BCM

The experimental literature on the role of congenital cone opsin deficiencies in mammals is limited and complex. Ideally, there should be a primate model with a human-like fovea with a high density of cones. Some monkeys are dichromats and may model color vision abnormalities (Neitz and Neitz, 2011) but there are no reports of cone cell reduction as we observed in our BCM cohort. An M-opsin null mutant rat has deficient cone function but there is neither cone loss nor outer segment abnormalities up to 12 months of age. This rat has also been suggested to be a model for common human color blindness (Xie *et al.,* 2010). Mice are dichromats with cones that may co-express both opsins (Applebury *et al*., 2000).

An S-cone opsin knockout mouse showed cone dysfunction and disordered or absent cone outer segments in the ventral retina (Daniele *et al*., 2011). A conclusion in this study of possible relevance to BCM is that cone photoreceptors, despite reduced cone opsin expression and abnormal cone outer segments, can survive for at least 1.5 years of this animal's life (Daniele *et al*., 2011). The results of the current human study point to the need for an animal model which would share sufficient characteristics with the BCM patients for proof-of-concept experiments en route to therapy.

Considerations for future clinical trials in BCM

A gene augmentation therapeutic approach for BCM due to deletion mutations must consider not only the potential for efficacy but also the fragility of these central retinas with residual foveal cone photoreceptors. Previous human trials using gene delivery by subretinal injection have documented loss of foveal outer segments and cone cells after this procedure (Maguire *et al*., 2008; Hauswirth *et al*., 2008; Jacobson *et al*., 2012). With the specter of further cone cell loss from subfoveal injections or even uncertainty about loss related to the procedure, it may be prudent to consider intravitreal administration of novel vectors, such as has been shown to be effective at transducing photoreceptors in recent reports in mice and at the fovea in a primate (Kay *et al*., 2013; Dalkara *et al*., 2013).

Candidate selection based on pre-enrollment imaging would also be necessary, considering the need to exclude those with macular atrophy. Further

research work on human BCM is also needed. It must be clarified whether BCM patients with other than deletion mutations are appropriate candidates to be included in future clinical trials aimed at treating residual central cones. A question not posed in the present study is whether the reduced cone cell layer and limited number of cone outer segments in the foveola of our patients can account for the reduced visual acuity. If there is a disproportionate vision loss for the number of residual cone photoreceptors, there is the possibility that the early loss of vision may also have a component of amblyopia or there may be abnormalities of post-receptor wiring in the retina and higher visual pathways (Baseler *et al.*, 2002). Expectations for efficacy based on a treatment-related increase in outer segment length or simply increased visual pigment content in cones with reduced outer segment length may have to be recalibrated adding in the uncertainty of a possible post-receptoral developmental acuity disturbance.

Adding further to the complexity of developing and interpreting outcomes of a BCM clinical trial are the constraints that light aversion imposes on psychophysical testing of cone function, except for measurement of absolute thresholds using chromatic stimuli. A potentially quantifiable parameter that may decrease with treatment is light aversion (for example, Gawande et al., 1989) and this may provide not only an outcome measure but also a practical benefit to these patients who otherwise show varying degrees of disability under ambient lights.

Acknowledgments

Supported by grants from BCMfamilies; Macula Vision Research Foundation; NIH P30EY001931, C06RR016511 and R01EY017607; Foundation Fighting Blindness (USA); Research to Prevent Blindness; Fight for Sight (UK); UK National Institute for Health Research (Moorfields Eye Hospital BRC) and Moorfields Special Trustees.

Author Disclosure statement

No competing financial interests exist.

References

Applebury, M.L., Antoch, M.P., Baxter, L.C., *et al.* (2000) The murine cone photoreceptor: a single cone type expresses both S and M opsins with retinal spatial patterning. Neuron, 27, 513-523.

Ayyagari, R., Kakuk, L.E., Coats, C.L., *et al.* (1999) Bilateral macular atrophy in blue cone monochromacy (BCM) with loss of the locus control region (LCR) and part of the red pigment gene. Mol. Vis. 5, 13.

Baseler, H.A., Brewer, A.A., Sharpe, L.T., *et al.* (2002) Reorganization of human cortical maps caused by inherited photoreceptor abnormalities. Nat. Neurosci. 5, 364-370.

Blackwell, H.R. and Blackwell, O.M. (1957) Blue mono-cone monochromacy: A new color vision defect. J. Optical Soc. Am. 47, 338.

Blackwell, H.R. and Blackwell, O.M. (1961) Rod and cone receptor mechanisms in typical and atypical congenital achromatopsia. Vision Res. 1, 62–107.

Borwein, B., Borwein, D., Medeiros, J. and McGowan, J.W. (1980) The ultrastructure of monkey foveal photoreceptors, with special reference to the structure, shape, size, and spacing of the foveal cones. Am. J. Anat. 159, 125-146.

Carroll, J., Dubra, A., Gardner, J.C., *et al.* (2012) The effect of cone opsin mutations on retinal structure and the integrity of the photoreceptor mosaic. Invest. Ophthalmol. Vis. Sci. 53, 8006-8015.

Carroll, J., Neitz, M., Hofer, H., *et al.* (2004) Functional photoreceptor loss revealed with adaptive optics: an alternate cause of color blindness. Proc. Natl. Acad. Sci. USA. 101, 8461-8466.

Carroll, J., Rossi, E.A., Porter, J., *et al.* (2010) Deletion of the X-linked opsin gene array locus control region (LCR) results in disruption of the cone mosaic. Vision Res. 50, 1989-1999.

Cho, K.I., Haque, M., Wang, J., *et al.* (2013) Distinct and atypical intrinsic and extrinsic cell death pathways between photoreceptor cell types upon specific ablation of Ranbp2 in cone photoreceptors. PLoS Genet. 9, e1003555.

Cideciyan, A.V., Swider, M., Aleman, T.S., *et al.* (2007) Reduced-illuminance autofluorescence imaging in ABCA4-associated retinal degenerations. J. Opt. Soc. Am. A. Opt. Image Sci. Vis. 24, 1457-1467.

Cideciyan, A.V., Zhao, X., Nielsen, L., *et al.* (1998) Mutation in the rhodopsin kinase gene slows recovery kinetics of rod and cone phototransduction in man. Proc. Natl. Acad. Sci. USA. 95, 328-333.

Cooper, R.F., Dubis, A.M., Pavaskar, A., *et al.* (2011) Spatial and temporal variation of rod photoreceptor reflectance in the human retina. Biomed. Opt. Express, 2, 2577-2589.

Crognale, M.A., Fry, M., Highsmith, J., Haegerstrom-Portnoy, G., *et al.* (2004) Characterization of a novel form of X-linked incomplete achromatopsia. Vis. Neurosci. 21, 197-203.

Curcio, C.A., Allen, K.A., Sloan, K.R., *et al.* (1991) Distribution and morphology of human cone photoreceptors stained with anti-blue opsin. J. Comp. Neurol. 312, 610-624.

Curcio, C.A., Sloan, K.R., Kalina, R.E. and Hendrickson, A.E. (1990) Human photoreceptor topography. J. Comp. Neurol. 292, 497-523.

Dalkara, D., Byrne, L.C., Klimczak, R.R., *et al.* (2013) In vivo-directed evolution of a new adeno-associated virus for therapeutic outer retinal gene delivery from the vitreous. Sci. Transl. Med. 5, 189ra76.

Daniele, L.L., Insinna, C., Chance, R., *et al.* (2011) A mouse M-opsin monochromat: retinal cone photoreceptors have increased M-opsin expression when S-opsin is knocked out. Vision Res. 51, 447-458.

Dubra, A., Sulai, Y., Norris, J.L., *et al.* (2011) Noninvasive imaging of the human rod photoreceptor mosaic using a confocal adaptive optics scanning ophthalmoscope. Biomed. Opt. Express 2, 1864-1876.

Gawande, A.A., Donovan, W.J., Ginsburg, A.P. and Marmor, M.F. (1989) Photoaversion in retinitis pigmentosa. Brit J Ophthalmol 73, 115-120.

Gibbs, D., Cideciyan, A.V., Jacobson, S.G. and Williams, D.S. (2009) Retinal pigment epithelium defects in humans and mice with mutations in MYO7A: imaging melanosome-specific autofluorescence. Invest. Ophthalmol. Vis. Sci. 50, 4386-4393.

Hauswirth, W.W., Aleman, T.S., Kaushal, S., *et al.* Treatment of leber congenital amaurosis due to RPE65 mutations by ocular subretinal injection of adeno-associated virus gene vector: short-term results of a phase I trial. Hum Gene Ther. 19, 979-990.

Helmholtz, H. von. (1866) Concerning the perceptions in general. In Treatise on physiological optics, vol. III, 3rd edn. Dover, New York, New York, USA.

Hendrickson, A. and Drucker, D. (1992) The development of parafoveal and mid-peripheral human retina. Behav. Brain Res. 49, 21-31.

Hendrickson, A., Possin, D., Vajzovic, L. and Toth, C.A. (2012) Histologic development of the human fovea from midgestation to maturity. Am. J. Ophthalmol. 154, 767-778.

Hofer, H., Carroll, J., Neitz, J., *et al.* (2005) Organization of the human trichromatic cone mosaic. J. Neurosci. 25, 9669-9679.

Humphries, M.M., Rancourt, D., Farrar, G.J., *et al.* (1997) Retinopathy induced in mice by targeted disruption of the rhodopsin gene. Nat Genet. 15, 216-219.

Humphries, M.M., Kenna, P.F., Campbell, M. *et al* (2012) C1q enhances cone photoreceptor survival in a mouse model of autosomal recessive retinitis pigmentosa. European Journal of Human Genetics. 20, 64-68.

Jacobson, S.G., Cideciyan, A.V., Ratnakaram, R., *et al.* (2012) Gene therapy for Leber congenital amaurosis caused by RPE65 mutations: safety and efficacy in 15 children and adults followed up to 3 years. Arch Ophthalmol. 130, 9-24.

Jonnal, R.S., Besecker, J.R., Derby, J.C., *et al.* (2010) Imaging outer segment renewal in living human cone photoreceptors. Opt. Express, 18, 5257-5257.

Kay, C.N., Ryals, R.C., Aslanidi, G.V., *et al.* (2013) Targeting photoreceptors via intravitreal delivery using novel, capsid-mutated AAV vectors. PLoS One, 8, e62097.

Kellner, U., Wissinger, B., Tippmann, S., *et al.* (2004) Blue cone monochromatism: clinical findings in patients with mutations in the red/green opsin gene cluster. Graefes Arch. Clin. Exp. Ophthalmol. 242, 729-735.

Kocaoglu, O.P., Lee, S., Jonnal, R.S., *et al.* (2011) Imaging cone photoreceptors in three dimensions and in time using ultrahigh resolution optical coherence tomography with adaptive optics. Biomed. Opt. Express, 2, 748-763.

Lem, J., Krasnoperova, N.V., Calvert, P.D., *et al.* (1999) Morphological, physiological, and biochemical changes in rhodopsin knockout mice. Proc. Natl. Acad. Sci. USA. 96, 736-741.

Leng, T., Marmor, M.F., Kellner, U., *et al.* (2012) Foveal cavitation as an optical coherence tomography finding in central cone dysfunction. Retina 32, 1411-1419.

Leveillard, T. and Sahel, J-A. (2010) Rod-derived cone viability factor for treating blinding diseases: from clinic to redox signaling. Science Translational Medicine, 2,1-5.

Liang, Y., Fotiadis, D., Maeda, T., *et al.* (2004) Rhodopsin signaling and organization in heterozygote rhodopsin knockout mice. J. Biol. Chem. 279, 48189-48196.

Lujan B.J., Roorda, A., Knighton, R.W. and Carroll, J. (2011) Revealing Henle's fiber layer using spectral domain optical coherence tomography. Invest. Ophthalmol. Vis. Sci. 52, 1486-1492.

Maguire, A.M., Simonelli, F., Pierce, E.A., *et al.* (2008) Safety and efficacy of gene transfer for Leber's congenital amaurosis. N. Engl. J. Med. 358, 2240-2248.

Makino, C.L., Wen, X.H., Michaud, N.A., *et al.* (2012) Rhodopsin expression level affects rod outer segment morphology and photoresponse kinetics. PLoS One 7, e37832.

Milam, A.H., Li, Z.Y. and Fariss, R.N. (1998) Histopathology of the human retina in retinitis pigmentosa. Prog. Retin. Eye Res. 17, 175-205.

Mizrahi-Meissonnier, L., Merin, S., Banin, E. and Sharon, D. (2010) Variable retinal phenotypes caused by mutations in the X-linked photopigment gene array. Invest. Ophthalmol. Vis. Sci. 51, 3884-3892.

Mustafi, D., Engel, A.H. and Palczewski, K. (2009) Structure of cone photoreceptors. Prog. Retin. Eye Res. 28, 289-302.

Mustafi, D., Kevany, B.M., Genoud, C., *et al.* (2011) Defective photoreceptor phagocytosis in a mouse model of enhanced S-cone syndrome causes progressive retinal degeneration. FASEB J. 25, 3157-3176.

Nathans, J., Davenport, C.M., Maumenee, I.H., *et al.* (1989) Molecular genetics of human blue cone monochromacy. Science 245, 831-838.

Nathans, J., Piantanida, T.P., Eddy, R.L., *et al.* (1986a) Molecular genetics of inherited variation in human color vision. Science 232, 203-210.

Nathans, J., Thomas, D. and Hogness, D.S. (1986b) Molecular genetics of human color vision: the genes encoding blue, green, and red pigments. Science 232, 193-202.

Neitz, J. and Neitz, M. (2011) The genetics of normal and defective color vision. Vision Res. 51, 633-651.

Osterberg, G. (1935) Topography of the layer of rods and cones in the human retina. Acta Ophthal. Supp. 6, 1–103.

Palczewski, K. (2010) Retinoids for treatment of retinal diseases. Trends Pharmacol. Sci. 31, 284-295.

Palczewski, K. (2012) Chemistry and biology of vision. J. Biol. Chem. 287, 1612-1619.

Rossi, E.A., Achtman, R.L., Guidon, A., *et al.* (2013) Visual function and cortical organization in carriers of blue cone monochromacy. PLoS One. 8, e57956.

Saari, J.C. (2000) Biochemistry of visual pigment regeneration: the Friedenwald lecture. Invest. Ophthalmol. Vis. Sci. 41, 337-348.

Sakami, S., Maeda, T., Bereta, G., *et al.* (2011) Probing mechanisms of photoreceptor degeneration in a new mouse model of the common form of autosomal dominant retinitis pigmentosa due to P23H opsin mutations. J. Biol. Chem. 286, 10551-10567.

Smith, V.C., Pokorny, J., Delleman, J.W., *et al.* (1983) X-linked incomplete achromatopsia with more than one class of functional cones. Invest. Ophthalmol. Vis. Sci. 24, 451-457.

Spaide, R.F. and Curcio, C.A. (2011) Anatomical correlates to the bands seen in the outer retina by optical coherence tomography: literature review and model. Retina 31, 1609-1619.

Srinivasan, V.J., Monson, B.K., Wojtkowski, M., *et al.* (2008) Characterization of outer retinal morphology with high-speed, ultrahigh-resolution optical coherence tomography. Invest. Ophthalmol. Vis. Sci. 49, 1571-1579.

Stockman, A., Sharpe, L.T. and Fach, C. (1999) The spectral sensitivity of the human short-wavelength sensitive cones derived from thresholds and color matches. Vision Res. 39, 2901-2927.

Syed, R., Sundquist, S.M., Ratnam, K., *et al.* (2013) High-resolution images of retinal structure in patients with choroideremia. Invest. Ophthalmol. Vis. Sci. 54, 950-961.

Tachibanaki, S., Tsushima, S. and Kawamura, S. (2001) Low amplification and fast visual pigment phosphorylation as mechanisms characterizing cone photoresponses. Proc. Natl. Acad. Sci. USA. 98, 14044-14049.

Ueyama, H., Muraki-Oda, S., Yamade, S., *et al.* (2012) Unique haplotype in exon 3 of cone opsin mRNA affects splicing of its precursor, leading to congenital color vision defect. Biochem. Biophys. Res. Commun. 424, 152-157.

Wang, J.S. and Kefalov, V.J. (2011) The cone-specific visual cycle. Prog. Retin. Eye Res. 30, 115-128.

Wang, Y., Macke, J.P., Merbs, S.L., *et al.* (1992) A locus control region adjacent to the human red and green visual pigment genes. Neuron 9, 429-440.

Weleber, R.G. (2002) Infantile and childhood retinal blindness: a molecular perspective (The Franceschetti Lecture). Ophthalmic Genet. 23, 71-97.

Xie, B., Nakanishi, S., Guo, Q., *et al.* (2010) A novel middle-wavelength opsin (M-opsin) null-mutation in the retinal cone dysfunction rat. Exp. Eye Res. 91, 26-33.

Youdelis, C. and Hendrickson, A.H. (1986) A qualitative and quantitative analysis of the human fovea during development. Vision Res. 26, 847-55.

Young, T. (1802) The Bakerian Lecture: On the theory of light and colours. Phil. Trans. R. Soc. 92, 12-48.

Figure Legends

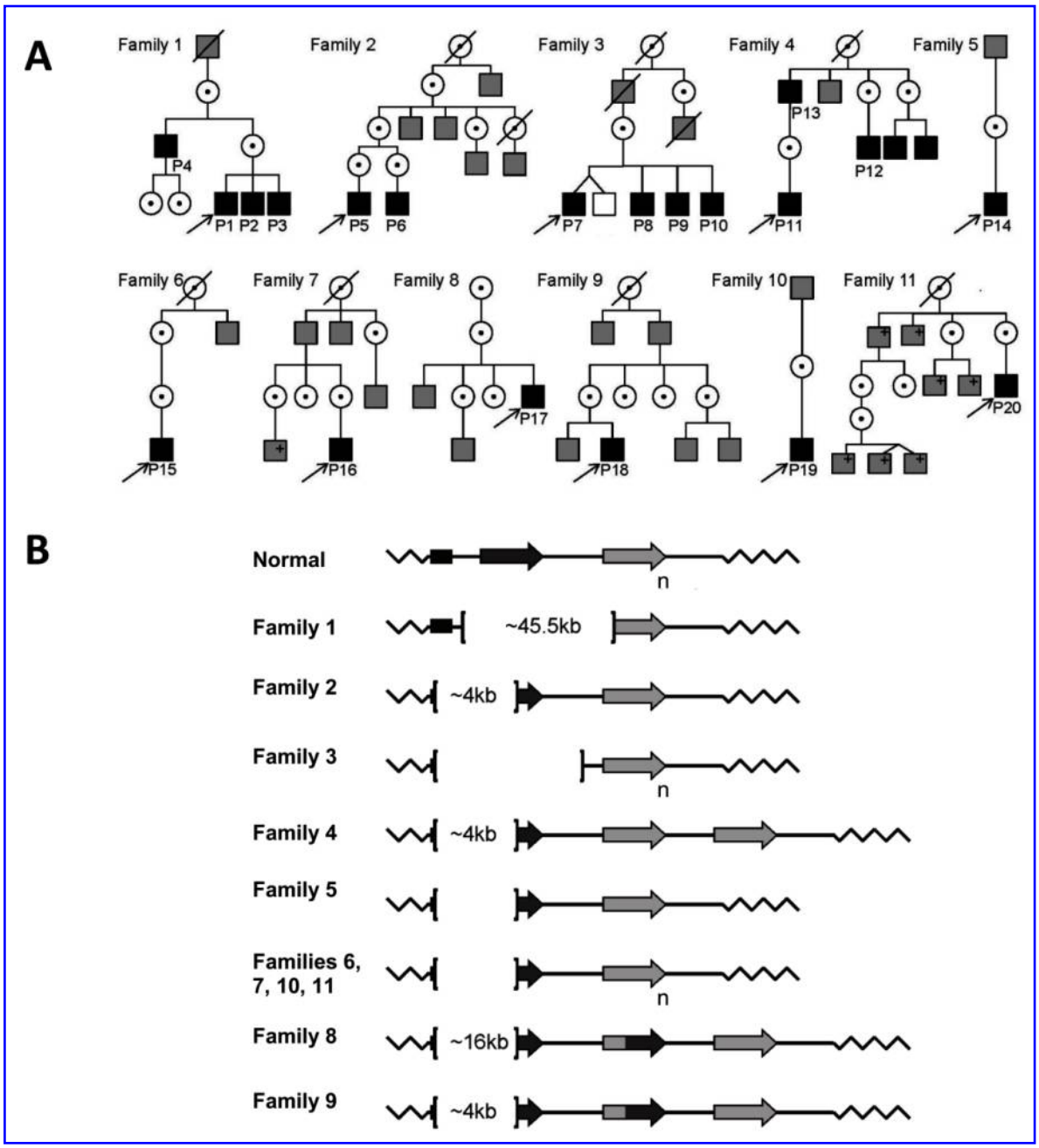

FIG.1. Pedigrees and genotypes of BCM families. (**A**) Pedigrees of the 11 families. Black filled squares, males diagnosed with BCM based on clinical evaluations and molecular testing; gray filled squares, affected males by history; +, positive for familial BCM mutation; unfilled squares, unaffected males by history; dotted circles, carrier females. (**B**) Schematic representation of BCM genotypes. In individuals with normal color vision, the X-chromosomal *OPN1LW/OPN1MW* gene array consists of a proximal long-wavelength

sensitive opsin (*OPN1LW*) gene (dark gray arrow), and one or more middle-wavelength sensitive opsin (*OPN1MW*) genes (light gray arrow) arranged in a head-to-tail tandem repeat. Subscript "n" indicates one or more M pigment genes. L/M hybrid genes are shown (dark/light gray arrow). Each gene is preceded by a proximal promoter and the expression is controlled by a single locus control region (LCR) upstream of the array (black rectangle). Genetic analyses implied that the *OPN1LW/OPN1MW* gene clusters in all patients of this study were impaired by large deletions affecting the locus control region (LCR) and varying parts of the opsin gene cluster with the exception of Family 1 which had an intact LCR with a deletion spanning the *OPN1LW* and *OPN1MW* genes. Brackets demarcate the deletions; deletion size is indicated inside the brackets where defined.

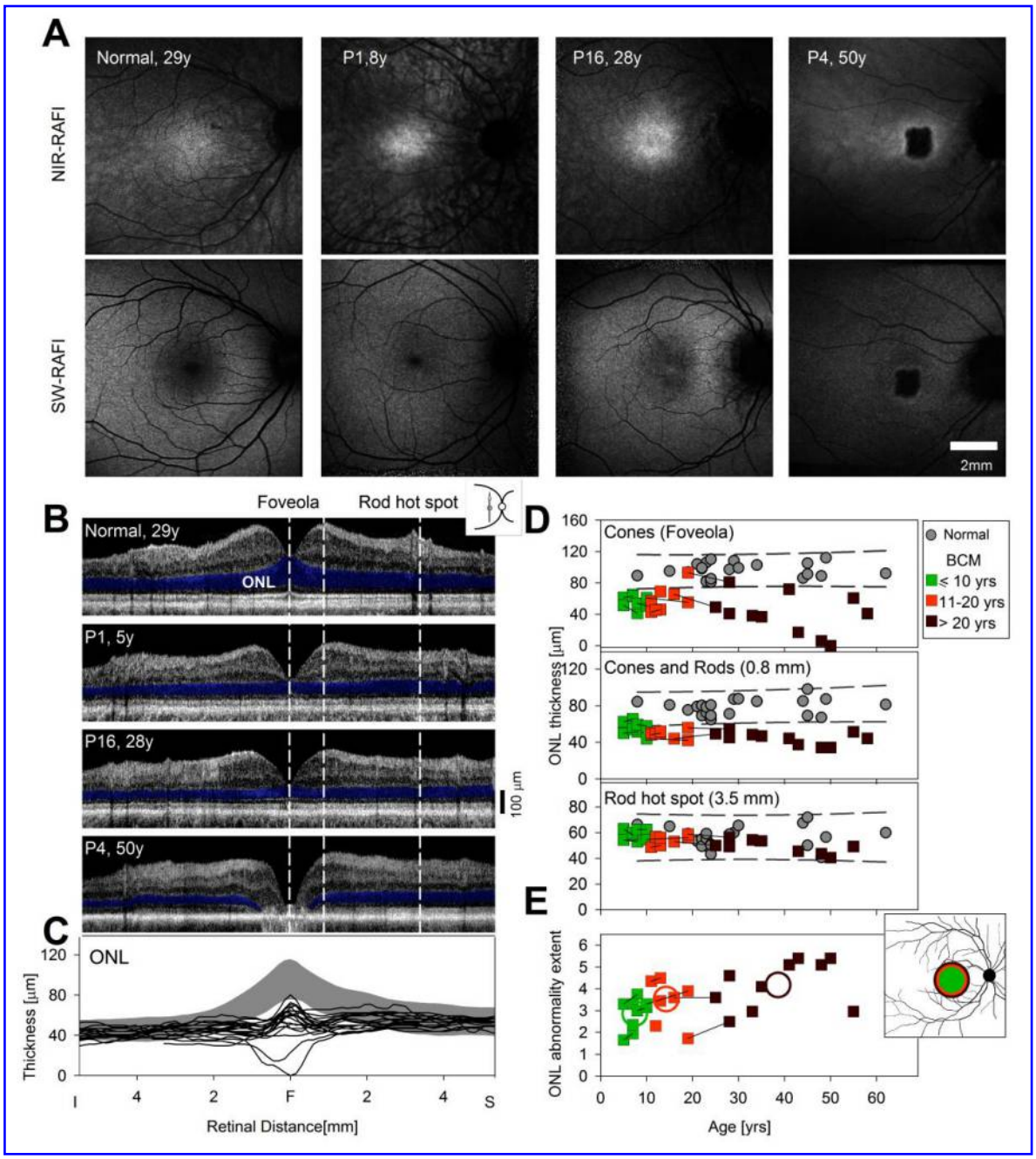

FIG.2. Younger BCM patients show normal RPE but abnormal thinning of the photoreceptor nuclear layer. (**A**) *En face* imaging of melanin and lipofuscin fluorophores of the RPE using NIR-RAFI and SW-RAFI, respectively, in a normal subject (age 29; myope, -6D) and 3 BCM patients. The small dark foveal region in the normal and P1 on SW-RAFI is the result of absorption of the excitation light by dense macular pigment; the larger dark region in the central macula of P4 on NIR-RAFI and SW-RAFI represents RPE atrophy. Retinal blood vessels and the optic nerve head (ONH) also appear darker than the

background. All images are shown contrast stretched for visibility of features. (**B**) Cross-sectional scans along the vertical meridian crossing the fovea in the same four eyes as shown in (A). ONL, where the photoreceptor nuclei reside, is highlighted (blue). Vertical dashed lines delineate the foveola dominated by cone photoreceptors, 0.8 mm superior retina with cone and rod photoreceptors, and the rod hot spot dominated by rod photoreceptors. (**C**) ONL thickness vertically across the central 10 mm of retina is graphically displayed for a group of normal subjects (gray represents mean±2SD; n=22; ages 8 to 62 years), and the BCM data (lines). (**D**) ONL thickness at the foveola (upper), 0.8 mm superior retina (middle) and the rod hot spot (lower) as a function of age in patients (colored symbols; green, ages <10; orange, ages 10-20; brown, ages >20 yrs) and normal controls (gray symbols). The 95% prediction interval of linear regression fit to the normal data is shown (gray dashed lines). Symbols connected with lines represent patients with multiple visits. (**E**) The extent of ONL abnormality along the vertical meridian as a function of age. Individual patient data are displayed as in panel (D). Average results for the three age groups are shown with colored circles. Inset, schematic of the average extent of ONL abnormality for the three age groups overlaid to scale on a representative retinal view.

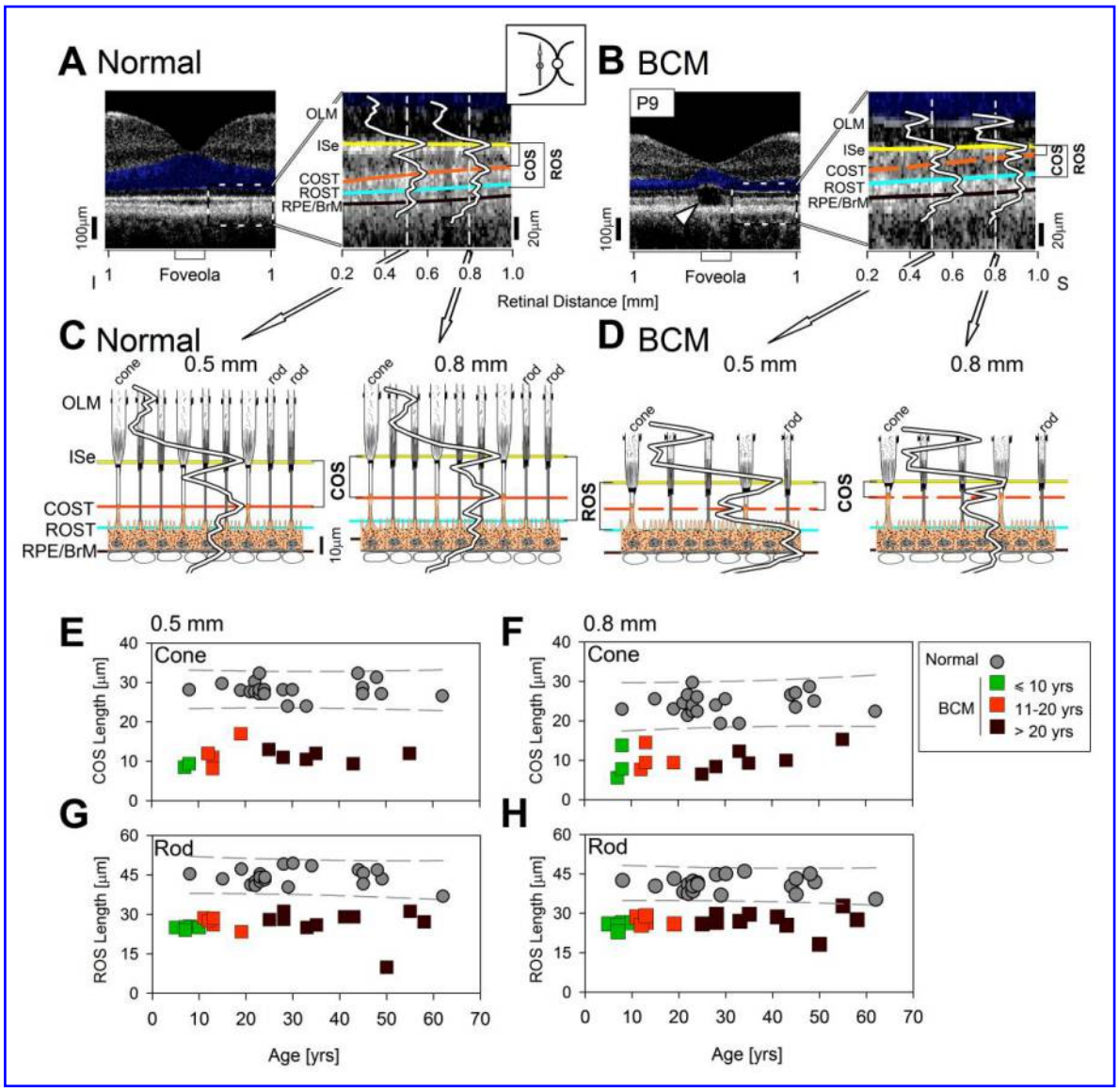

FIG.3. Abnormal cone and rod photoreceptor outer segments in BCM. (**A,B**) *Left panels.* An OCT along the vertical meridian in a representative normal (A) and BCM patient P9 (B). *Right panels.* Enlarged view of the region immediately superior to the foveola. Four of the five hyperscattering bands are painted for visibility: ISe (yellow), COST (orange), ROST (cyan) and RPE/BrM (brown). OLM layer is also labeled. LRPs are shown at 0.5 and 0.8 mm eccentricity. Dashed orange line in the BCM patient represents intermittent visibility of the COST peak. 'Cavitation' in P9 causes structural loss of the ISe and distal layers at the foveola (arrowhead). The lengths of ROS and COS are bracketed. (**C,D**) LRPs from the two regions (0.5 and 0.8 mm superior) are overlaid onto models of retina showing the region at rod and cone inner and outer segments and the RPE. Axial dimensions are to

scale but lateral dimensions are not. (**E-H**) COS and ROS lengths at the 0.5 and 0.8 mm superior retina as a function of age in patients. Individual patient symbols and colors as in Fig.2. Individual normal controls (gray symbols), and the 95% prediction interval of linear regression fit to the normal data (gray dashed lines) are shown.

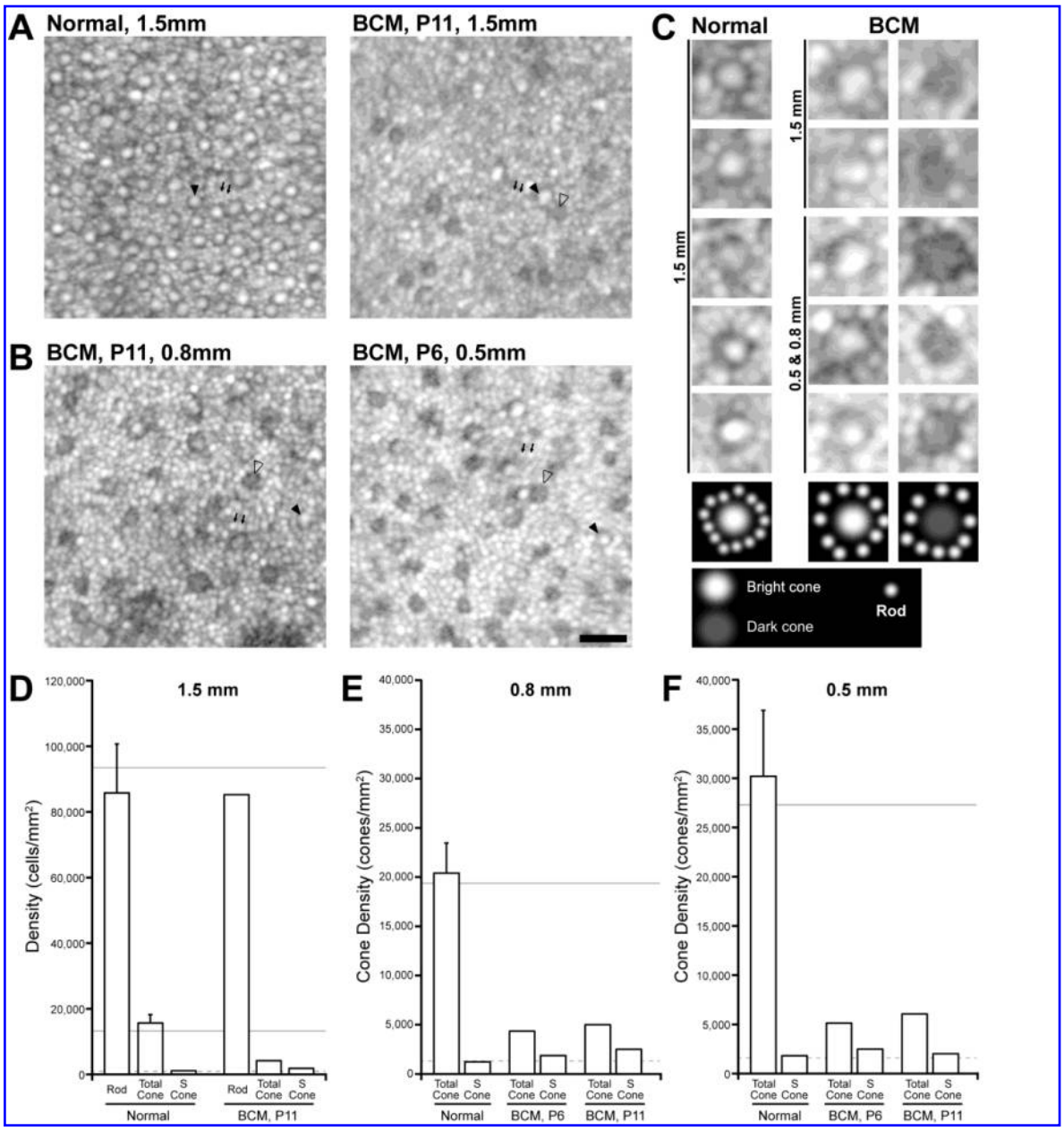

FIG. 4. Residual cone structure in BCM. (**A**) The photoreceptor mosaic visible with AOSLO at superior retina 1.5 mm eccentric to the fovea in a normal subject and P11. Normal (left) shows larger regularly spaced spots representing cones (filled arrowhead) with more numerous, smaller rods (small arrows) interleaved across the mosaic. In comparison, P11 (right) shows a different pattern of bright cones with normal reflectivity (filled arrowhead) and dark cones with impaired/diminished reflectivity (unfilled arrowhead), and more numerous smaller rods (small arrows). (**B**) The photoreceptor mosaic in two BCM patients at 0.8 and 0.5 mm eccentricity also showed rods along with two populations

of cones. Scale bar= 20 um. (**C**) Enlarged examples of normal and BCM structures at different eccentricities. Schematic drawings (lowest panel) define the interpretation assigned to the intensity patterns observed. Normally waveguiding/reflecting bright cones have a characteristic reflectance profile (bright center with a dark ring and adjacent rods). Dark cones have a substantially reduced or missing central reflective component. (**D-F**) Quantitative measurements of rod and/or cone density derived from the AOSLO images (open bars), compared to previous estimates from histology (solid horizontal lines). Error bars are 1 std. The dashed line indicates the expected (mean normal) S cone density, assuming S-cones comprise between 6-7% of the total normal cone population. In all cases, the patients with BCM had a lower cone density than that seen in normals, but a higher total cone density than would be expected for just the S cone submosaic, indicating at least some of the cones in these images are L/M cones.

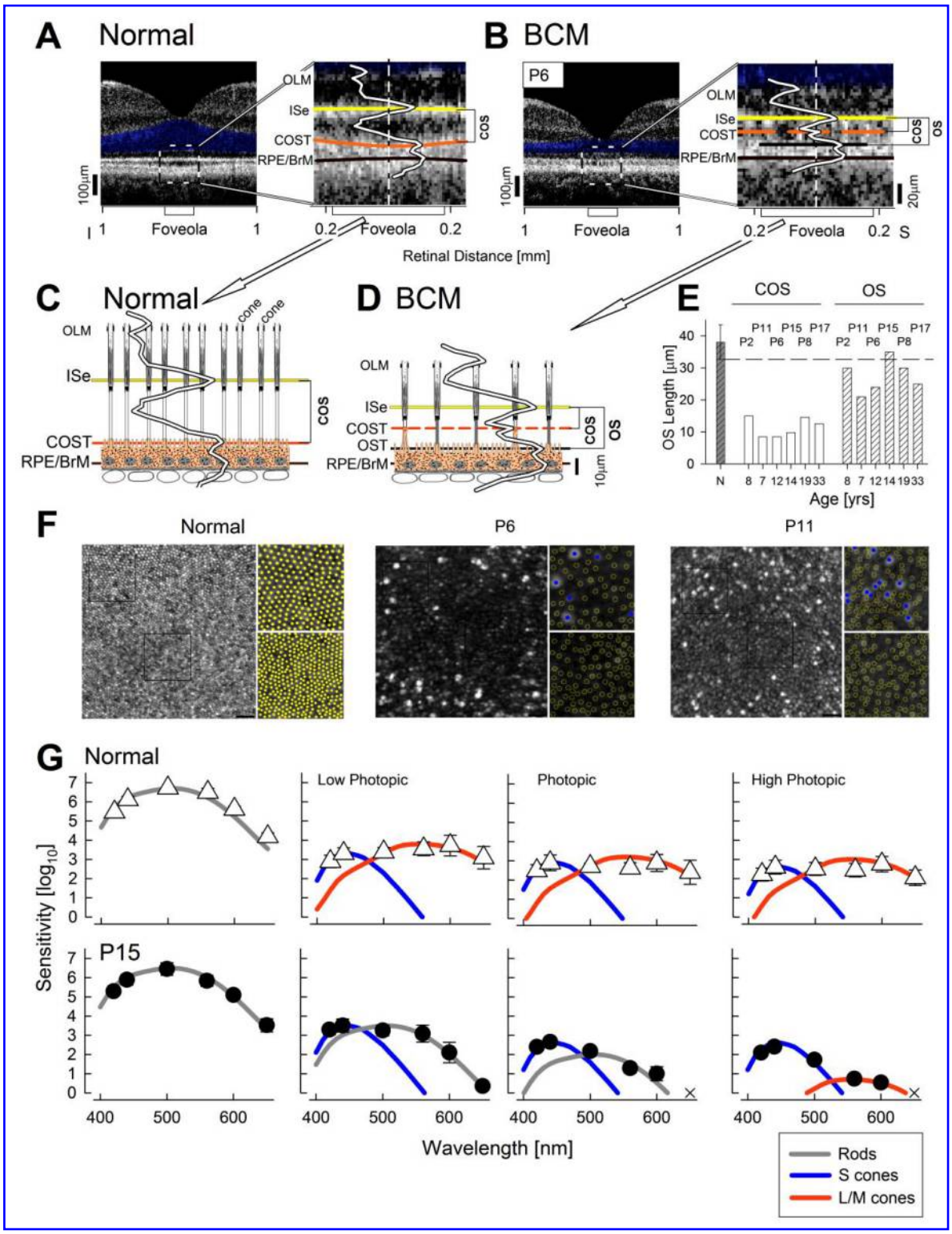

FIG. 5. Photoreceptor inner and outer segments at the BCM foveola, and evidence of red/green cone-mediated visual function. (**A,B**) *Left panels.* An OCT along the vertical meridian in a representative normal subject (A) and BCM P6 (B). *Right panels.* Enlarged

view of the foveolar region. Hyperscattering bands are painted for visibility as in Fig.3. The additional hyperscattering band at the BCM foveola is painted black. LRPs are overlaid. The lengths of COS and the additional OS in the BCM patient are bracketed. (**C,D**) LRPs are overlaid onto models of foveolar retina showing only cones in the normal (C) and a mixture of cones and another cell type in the BCM (D). Axial dimensions are to scale but lateral dimensions are not. (**E**) Histograms of OS length measurements at the foveola of 6 BCM patients who lacked large cavitations. Shorter COS lengths and longer OS lengths are grouped; ages and patient numbers are specified. Hashed gray bar to left represents mean (+/-2SD) COS length for the normal (N). (**F**) The photoreceptor mosaic visible with AOSLO at the foveola in a normal subject compared to BCM patients P6 and P11. Normal (left) shows a contiguous mosaic of cones decreasing in size and increasing in density towards the center of the foveola. In comparison, P6 and P11 show a disrupted foveal mosaic made up of a central region of photoreceptors with a reduced density and reflectivity compared to normal and a surrounding 'ring' of highly reflective bright photoreceptors. Square insets for each panel show an image from ~0.1 mm from the foveal center (top) and an image at the foveal center (bottom). In the normal, it is not possible to determine the spectral subtype of the cones in these images, which are marked as filled yellow circles. In P6 and P11, the S-cones are marked as filled blue circles, while the weakly reflective structures are marked as open yellow circles. Scale bar= 20 μm. (**G**) Spectral sensitivity functions in normal subjects and BCM patient P15 at a retinal location centered at 0.6 mm eccentric to the foveola. Scotopic conditions recorded under dark-adaptation; photopic conditions recorded on steady achromatic lights increasing from 1 to 20 $cd.m^{-2}$. Theoretical functions describing rod (gray), S cone (blue), L/M cone (orange) sensitivities are shown after vertical shifts to fit relevant normal and BCM data. X marks the stimuli not seen by the patient.

Supplementary Data

Human cone visual pigment deletions spare sufficient photoreceptors to warrant gene therapy

Artur V. Cideciyan, Robert B. Hufnagel, Joseph Carroll, Alexander Sumaroka, Xunda Luo, Sharon B. Schwartz, Alfredo Dubra, Megan Land, Michel Michaelides, Jessica C. Gardner, Alison J. Hardcastle, Anthony T. Moore, Robert A. Sisk, Zubair M. Ahmed, Susanne Kohl, Bernd Wissinger, and Samuel G. Jacobson

Supplemental Methods

Genetic Analyses.

Whole venous blood samples were collected and genomic DNA extracted according to standard procedures. The structure and integrity of the *OPN1LW*/*OPN1MW* gene cluster on the X-chromosome were investigated by three methods, representing different groups of authors: Method 1 (performed by SK, BW in 12 of the 20 patients; Patients 1-4,7-10,15,16,19, 20) used a two-tiered testing scheme. A first-tier screened for large genomic deletions at the *OPN1LW*/*OPN1MW* gene cluster and the upstream locus control region (LCR), the presence of single or multiple opsin gene copies, and the presence or absence of the common point mutation c.607T>C p.C203R. Briefly, duplex polymerase chain reactions (PCRs) including primers for the tested fragment and an autosomal control fragment were performed for: 1) a sequence defined as the common overlap of known deletions of the LCR (Nathans *et al*., 1989; Nathans *et al*., 1993) the *OPN1LW* promoter; and 3) the *OPN1MW* promoter to test for large genomic deletions and the presence of single or multiple opsin gene copies. In addition, two PCR fragments for exons 4 and 5, respectively, for both *OPN1LW* and *OPN1MW* were amplified and digested with B*stUI* and R*sal*, respectively. The

restriction fragment length polymorphism (RFLP) in exon 4 via B*stUI* analysed for the c.607T>C p.C203R mutation, while the RFLP in exon 5 via R*saI* addressed the dimorphism at amino acid position 277 – p.Y277 being specific for the *OPN1LW* gene, and p.F277 for the *OPN1MW* gene. Second-tier testing (not necessary for the cases reported in this study) analyzed for other deleterious point mutations or haplotypes in cases with either single or multiple structurally intact gene copies. Primers and conditions are available upon request.

In Method 2 (performed by RH, ZA in 7 of the 20 patients; Patients 5,6,11-13,17,18) there was sequencing of the LCR, promoter, and *OPN1MW* and *OPN1LW* genes. Primers flanking 300-500bp segments were designed to amplify exons, the immediate 500bp of 5' promoter, the 37bp core LCR sequence, interval sequences spaced every ~1kb from the promoter to ~9kb upstream of the first opsin gene. PCR and DNA sequencing was performed as described (Jaworek *et al*., 2012). Briefly, PCR products were amplified using 50ng DNA, with standard PCR reagents (Genscript) or AmpliTaq gold (Invitrogen), on an ABI Veriti Thermocycler (Applied Biosystems, Austin, TX). A portion of amplified products were electrophoresed and measured on a 2% agarose gel. PCR products were precipitated and sequencing PCR performed using BigDye Terminator Ready Reaction Mix (ABI Biosystems). PCR primer sequences and conditions are available upon request. To evaluate for deletions, the presence or absence of PCR products was checked - spaced every ~1kb of the 9kb region upstream of the first opsin gene. Deletion size was estimated by the absence of sequential PCR products (assumed to be encompassed by the deletion). To confirm the absence

of the LCR, three overlapping primer pairs were designed to amplify the core 37kb segment and surrounding LCR. Deletion endpoints were mapped by designing forward and reverse primers flanking the region of the absent PCR products. Real time PCR (RT-PCR) was used to determine the number of genes in the array, and the order or *OPN1LW* and *OPN1MW* genes was determined (Neitz and Neitz, 2011). Briefly, a quantitative RT-PCR assay was employed to estimate the relative ratio of first versus downstream genes in the X-chromosome opsin gene arrays. Quantitative RT-PCR was also used to estimate the relative ratio of L to M genes in each X-chromosome array.

Method 3 (performed by JCG, AJH in P14) has been described (Gardner et al., 2010).

In Vivo Microscopy of Human Retina.

Cross-sectional images of the retina were obtained with a spectral-domain optical coherence tomography (SD-OCT) instrument (RTVue-100, Optovue Inc., Fremont, CA). Overlapping, non-averaged, 9 mm-length scans were used to study the retina along the vertical meridian through the fovea. Raster scans (6x6 mm, 101 lines with 513 longitudinal reflectivity profiles [LRPs] each) centered at the fovea provided high density coverage of the macula. Scans were analyzed with custom programs (MatLab 7.5; MathWorks, Natick, MA). For the outer retinal sublaminae, signal peak assignments were based on our previously published work (Aleman *et al.,* 2008; Jacobson *et al.,* 2009; Maeda *et al*., 2009; Cideciyan *et al*., 2011; Sakami *et al*., 2011; Jacobson *et al.,* 2013) and those of others (Hood *et*

al., 2009; Zhang *et al.,* 2011; Birch *et al.,* 2013) consistent with hypotheses on the correspondence between OCT signals and histologically-defined layers (Huang *et al.,* 1998; Jacobson *et al.,* 2003; Spaide and Curcio, 2011) and interpretations of ultra-high resolution AO OCT scans (Kocaoglu *et al.,* 2011). Specifically, outer retinal sublaminae were assumed to include: a) a hyperreflective layer at the outer plexiform layer (OPL); b) a hyporeflective layer at the outer nuclear layer (ONL); c) a hyperreflective layer at the outer limiting membrane (OLM); d) a hyperreflective layer near the junction of inner and outer segments possibly corresponding to the ellipsoid region of inner segments (ISe); e) a hyperreflective layer near the interface between cone outer segments (COS) and contact cylinder (extra-foveal) or apical processes (foveal) of the RPE; f) a hyperreflective layer near the interface between rod outer segments (ROS) and RPE apical processes; and g) a hyperreflective layer near the interface between basal RPE and Bruch membrane. Layer (f) could merge into layer (e) and become a single layer at the foveola in normal subjects. ONL thickness was defined as the distance from (a) to (c), COS thickness from (d) to (e), and ROS thickness from (d) to (f). Normal subjects (n=22; ages 8 to 62 years) included a subset (n=15) with spherical errors +2 to -4 D, and another subset (n=7) with high myopia, -5 to-10 D.

Adaptive Optics Imaging of the Photoreceptor Mosaic.

A previously described adaptive optics scanning laser ophthalmoscope (AOSLO) was used to image each subject's photoreceptor mosaic (Dubra and Sulai, 2011). Image sequences of 150 frames were recorded at each retinal

location using a 775 nm or 796 nm superluminescent diode, and an internal fixation target was used to guide the subjects' fixation for imaging of different retinal locations. Intra-frame distortion due to the sinusoidal motion of the resonant optical scanner was estimated from images of a Ronchi ruling and subsequently removed by resampling each frame of the raw video over a square pixel grid. After desinusoiding, a reference frame with minimal intra-frame eye motion was manually selected from each image sequence for subsequent registration using a previously described strip-based registration method (Dubra and Harvey, 2010). Each frame was divided into strips and each strip was registered against the reference frame by finding the relative position that maximized the normalized cross-correlation between them (Dubra and Harvey, 2010). The registered frames were then averaged to create a single high signal to noise image for each image sequence, with between 40 and 50 frames being averaged to produce the final image at each retinal location.

The registered images for each subject were combined into a single montage (Adobe Photoshop; Adobe Systems, Inc., San Jose, CA), which was then registered to an image of the fundus exported from the Cirrus HD-OCT system (Carl Zeiss Meditec, Dublin, CA). This was done to determine the absolute location of the individual images within the montage with respect to the fovea. Axial length measurements were obtained for all subjects using an IOL Master (Carl Zeiss, Inc, Dublin, CA USA). Normal subjects (n=17; ages 20 to 36 years; axial length 22.46-27.98 mm) were imaged as controls: 11 were imaged at 0.5 and 0.8 mm, four

were imaged at 1.5 mm, one was imaged at all three parafoveal locations, and one was imaged at the foveal center and 0.5 and 0.8mm.

For 13 of the controls and two patients (P6, P11), cone density was measured at 0.5 and 0.8 mm superior to the fovea using manual selection of cones; and in five of the controls and one of the patients (P11), both cone and rod density was measured at 1.5 mm. In the parafovea, density was measured over an 80 μm x 80 μm sampling window, which was chosen because the cone mosaic was relatively sparse in the two patients, and it was necessary to use a sampling window large enough to avoid capturing local inhomogeneity of the residual cone mosaic.

Spectral Sensitivity Function.

Spectral sensitivity functions were measured in normals (n=3, ages 31-50) and BCM P15 using a modified perimeter with methods previously described (Cideciyan *et al.*, 1997, 1998, 2000; Jacobson *et al.*, 2013). In brief, a 1.7° (equivalent to ~0.5 mm on the retina) diameter, 200-ms duration test stimulus spectrally shaped by interference filters (7 nm to 12 nm full-width at half-maximum, depending on wavelength) was used. In normal subjects, stimuli were presented at 0.6 mm superior retina with the use of an offset dim fixation. In BCM, stimuli were presented at the center of four dim fixation lights. Thresholds are reported normalized to energy. Spectral sensitivity functions for rods, S and L/M cones are also shown in term of relative energy. Spectral sensitivity functions were recorded under dark-adapted conditions and on increasing levels of achromatic

backgrounds. Sensitivities were fit by eye with scotopic and photopic luminosity functions, and S cone spectral sensitivity function (Stockman *et al.*, 1999). Note that normal subtractive cone-cone interactions on brighter background lights cause relative reduction of the sensitivity to the 560 nm stimulus as compared to neighboring 500 and 600 nm samples (Sperling and Harwerth, 1971).

References

Aleman, T.S, Cideciyan, A.V., Sumaroka, A., *et al.* (2008) Retinal laminar architecture in human retinitis pigmentosa caused by rhodopsin gene mutations. Invest. Ophthalmol. Vis. Sci. 49, 1580-1590.

Birch, D.G., Locke, K.G., Wen, Y., *et al.* (2013) Spectral-Domain optical coherence tomography measures of outer segment layer progression in patients with X-Linked retinitis pigmentosa. JAMA Ophthalmol. [Epub ahead of print]

Cideciyan, A.V., Haeseleer, F., Fariss, R.N., *et al*. (2000) Rod and cone visual cycle consequences of a null mutation in the 11-cis-retinol dehydrogenase gene in man. *Vis. Neurosci.* 17, 667-678.

Cideciyan, A.V., Pugh, E.N. Jr., Lamb, T.D., *et al.* (1997) Rod plateaux during dark adaptation in Sorsby's fundus dystrophy and vitamin A deficiency. Invest. Ophthalmol. Vis. Sci. 38, 1786-1794.

Cideciyan, A.V., Rachel, R.A., Aleman, T.S., *et al.* (2011) Cone photoreceptors are the main targets for gene therapy of NPHP5 (IQCB1) or NPHP6 (CEP290) blindness: generation of an all-cone Nphp6 hypomorph mouse that mimics the human retinal ciliopathy. Hum. Mol. Genet. 20,1411-1423.

Cideciyan, A.V., Zhao, X., Nielsen, L., *et al.* (1998) Null mutation in the rhodopsin kinase gene slows recovery kinetics of rod and cone phototransduction in man. *Proc. Natl. Acad. Sci. USA.* 95, 328-333.

Dubra, A. and Harvey, Z. (2010) Registration of 2D images from fast scanning ophthalmic instruments. The 4th International Workshop on Biomedical Image Registration.

Dubra, A. and Sulai, Y. (2011) Reflective afocal broadband adaptive optics scanning ophthalmoscope. *Biomed. Opt. Express* 2, 1757-1768.

Gardner, J.C., Webb, T.R., Kanuga, N., *et al.* (2010) X-linked cone dystrophy caused by mutation of the red and green cone opsins. Am J. Hum. Genet. 87, 26-39.

Hood, D.C., Lin, C.E., Lazow, M.A., *et al.* (2009) Thickness of receptor and post-receptor retinal layers in patients with retinitis pigmentosa measured with frequency-domain optical coherence tomography. Invest. Ophthalmol. Vis. Sci. 50, 2328-2336.

Huang, Y., Cideciyan, A.V., Papastergiou, G.I., *et al.* (1998) Relation of optical coherence tomography to microanatomy in normal and rd chickens. Invest. Ophthalmol. Vis. Sci. 39, 2405-2416.

Jacobson, S.G., Aleman, T.S., Sumaroka, A., *et al.* (2009) Disease boundaries in the retina of patients with Usher syndrome caused by MYO7A gene mutations. Invest. Ophthalmol. Vis. Sci. 50, 1886-1894.

Jacobson, S.G., Cideciyan, A.V., Aleman, T.S., *et al.* (2003) Crumbs homolog 1 (CRB1) mutations result in a thick human retina with abnormal lamination. Hum. Mol. Genet. 12, 1073-1078.

Jacobson, S.G., Cideciyan, A.V., Peshenko, I.V., *et al.* (2013) Determining consequences of retinal membrane guanylyl cyclase (RetGC1) deficiency in human Leber congenital amaurosis en route to therapy: residual cone-photoreceptor vision correlates with biochemical properties of the mutants. Hum. Mol. Genet. 22, 168-183.

Jaworek, T.J., Kausar, T., Bell, S.M., *et al.* (2012) Molecular genetic studies and delineation of the oculocutaneous albinism phenotype in the Pakistani population. Orphanet J. Rare. Dis. 7, 44.

Kocaoglu, O.P., Lee, S., Jonnal, R.S., *et al.* (2011) Imaging cone photoreceptors in three dimensions and in time using ultrahigh resolution optical coherence tomography with adaptive optics. Biomed. Opt. Express 2, 748-763.

Maeda, T., Cideciyan, A.V., Maeda, A., *et al.* (2009) Loss of cone photoreceptors caused by chromophore depletion is partially prevented by the artificial chromophore pro-drug, 9-cis-retinyl acetate. Hum. Mol. Genet. 18, 2277-2287.

Nathans, J., Davenport, C.M., Maumenee, I.H., *et al.* (1989) Molecular genetics of human blue cone monochromacy. Science, 245, 831-838.

Nathans, J., Maumenee, I.H., Zrenner, E., *et al.* (1993) Genetic heterogeneity among blue-cone monochromats. Am. J. Hum. Genet. 53, 987-1000.

Neitz, J. and Neitz, M. (2011) The genetics of normal and defective color vision. Vision Res. 51, 633-651.

Sakami, S., Maeda, T., Bereta, G., *et al.* (2011) Probing mechanisms of photoreceptor degeneration in a new mouse model of the common form of autosomal dominant retinitis pigmentosa due to P23H opsin mutations. J. Biol. Chem. 286, 10551-10567.

Spaide, R.F. and Curcio, C.A. (2011) Anatomical correlates to the bands seen in the outer retina by optical coherence tomography: literature review and model. *Retina* 31, 1609-1619.

Sperling, H.G. and Harwerth, R.S. (1971) Red-green cone interactions in the increment-threshold spectral sensitivity of primates. *Science* 172, 180-184.

Stockman, A., Sharpe, L.T. and Fach, C. (1999) The spectral sensitivity of the human short-wavelength sensitive cones derived from thresholds and color matches. *Vision Res.* 39, 2901-2927.

Zhang, X., Ramachandran, R., Talamini, C.L., *et al.* (2011) The inner segment/outer segment border seen on optical coherence tomography is less intense in patients with diminished cone function. Invest. Ophthalmol. Vis. Sci. 52, 9703-9709.

TABLE 1. CLINICAL CHARACTERISTICS OF THE BCM PATIENTS

Patient/ Family	*Age at visits (y)*	*Visual acuity*[a]	*Refraction*[b]	*Nystagmus (in early life)*[c]	*Light aversion*	*Color vision (confusion axis)*[d]	*S-cone function*[e]	*ERG*[f] *amplitude*	
								Rod b-wave	*Cone flicker*
P1/F1	5,8	20/100	-12.50	+ (2-3 mos)	+	protan-deutan	+	← np →	
P2/F1	8,10	20/80	-3.75	+ (2-3 mos)	+	protan-deutan	+	← np →	
P3/F1	11,13	20/63	-12.75	+ (2-3 mos)	+	protan-deutan	+	← np →	
P4/F1	48,50	20/100	-10.25	+ (infancy)	+ (disabling)	protan-deutan	+	N	A
P5/F2	7	20/100	-3.25	+ (3-4 mos), ↑(12 mos), ↓(2.5 yr)	+	protan-deutan	+	N(b)	A
P6/F2	12	20/100	-5.00	+ (9 mos), ↓(18 mos), ↓↓(4 yr)	+ (not prominent)	protan-deutan	+	← np →	
P7/F3	5,7	20/250	-0.50	+	no complaints	all three axes	+	N	A
P8/F3	10,19	20/100	-5.00	+ (4 mos)	no complaints	protan-deutan	+	← np →	
P9/F3	16,25	20/100	-6.00	+ (6 mos)	+ (disabling)	protan-deutan	np	N	A
P10/F3	19,28	20/125	-6.50	+ (10 mos)	+	protan-deutan	+	N	A
P11/F4	7	20/80	+2.00	+	+	protan-deutan	np	N	A
P12/F4	41	20/160	-13.00	+	+	np	np	← np →	
P13/F4	58	20/200	-10.00	+	+	np	np	N	A
P14/F5	11	20/100	-7.50	+ (infancy)	+	protan-deutan	+	N(b)	A
P15/F6	14	20/100	-4.00	+ (3 mos)	no complaints	protan-deutan	+	N	A
P16/F7	28	20/125	-8.50	+ (<1 yr), ↓(later in life)	+ (disabling)	protan-deutan	+	N	A
P17/F8	33	20/100	-3.75	+	+ (disabling)	protan-deutan	+	← np →	
P18/F9	35	20/63	-5.50	+	+ (disabling)	protan-deutan	+	N(b)	A
P19/F10	43	20/80	-6.00	+ (minimal)	glare	deutan	+	N	A
P20/F11	55	20/80	-6.50	+	+ (disabling)	all three axes	+	← np →	

np, not performed; +, present.

[a]Best corrected visual acuity at most recent visit; similar in the two eyes.

[b]Spherical equivalent; average of both eyes.

[c]Ages when nystagmus was first noted or when changed, amplifying the comment 'in early life' when possible. The ages cited are from historical accounts by patients or parents (mos, months; yr, years). Arrows indicate whether there was recalled reduction or increase (and at what age).

[d]Farnsworth D-15 color panel result.

[e]Detection of 440 nm target on 100 phot.cd/m^2 yellow background, or detectable S-cone ERG.

[f]Electroretinography was performed in different laboratories with different electrode types, protocols and normal limits. N, within normal limits of the laboratory; N(b), borderline normal - reports indicated blink or nystagmus artifact, imperfect cooperation, head not completely within ganzfeld stimulus or other possible sources of reduced amplitude. A, abnormal.